Electronic Supplementary Material (ESI) for Energy Advances.
This journal is © The Royal Society of Chemistry 2024

Supporting Information

Single-membrane pH-decoupling Aqueous Battery Using Proton-coupled Electrochemistry for pH Recovery

Dawei Xi[1], Zheng Yang[1], Abdulrahman M. Alfaraidi[1], Yan Jing[2], Roy G. Gordon[1,2], Michael J. Aziz[1,*]

1 John A. Paulson School of Engineering and Applied Sciences, Harvard University, Cambridge, MA, USA.

2 Department of Chemistry and Chemical Biology, Harvard University, Cambridge, MA, USA

Materials and methods

Materials and Synthesis

4,4′-bis(hydroxymethyl)-2,2′-bipyridine (Bhmbpy), manganese (II) acetate, acetic acid (HOAc), sodium acetate (NaOAc), Poly (acrylic acid) sodium salt (NaPAA, average MW 2000), NaCl, NaBr, NaOH, $ZnBr_2$, $FeCl_2$ were purchased from VWR International. (((9,10-dioxo-9,10-dihydroanthracene-2,6-diyl)bis(oxy))bis(propane-3,1-diyl))bis(phosphonic acid) (2,6-DPPEAQ) was purchased directly from TCI Chemicals. Fumasep® E-620K and Nafion® 212 as cation exchange membrane, and Selemion® DSV-N anion exchange membrane were purchased and only soaked in 1M NaCl or KCl solution before usage. 5 mg cm^{-2} Pt gas diffusion electrode (GDE) was purchased from fuel cell store.

1,4-BTMAPAQ was synthesized by mixing 40 mmol of dihydroxyanthraquinone, 88 mmol of anhydrous K_2CO_3, and 9.5 mmol of KI in 160 mL of anhydrous DMF. After stirring for 10 min, 88 mmol of 3-bromopropyl trimethylammonium bromide was introduced. The resulting dark mixture was sealed to exclude moisture and then stirred vigorously at 100 ˚C for 16 hours. 150 mL of ethyl acetate was added to the slurry after cooling, and then filtered to isolate a brown solid. The solid was dissolved in methanol, filtered to remove most of the inorganic salts. Filtrate was collected and evaporated until dry. The product was then dissolved in water and used an anion-exchange resin column to exchange bromide ions into chloride ions. This red solid was then dissolved in methanol to form a saturated solution, which was gradually added to 200 mL of ethyl acetate. Precipitates were collected by filtration to obtain the orange product.

$Fe(Bhmbpy)_3$ electrolyte was prepared by dissolving $FeCl_2$ (0.1 M) and Bhmbpy (0.35 M) with a ratio of 1:3.5 in 1 M NaCl, using HCl adjusting pH to 3. BTMAPAQ electrolyte was prepared by dissolving 1,4-BTMAPAQ (0.1 M) in 1 M NaCl, using NaOH adjusting pH to 12, if not claimed otherwise.

DPPEAQ electrolyte was prepared by dissolving 2,6-DPPEAQ (0.25 M) in 0.5 M NaCl, using NaOH adjusting pH to 12. NaBr electrolyte was prepared by dissolving NaBr (1 M) in water, then adding NaPAA (0.5 M sodium), adding 0.25 M HBr and 0.1 M Br_2.

$Mn(OAc)_2$ electrolyte was prepared by dissolving 1 M $Mn(OAc)_2$ in 3 M HOAc, adding 1 M NaOAc, 0.05 M KI. $Na_2Zn(OH)_4$ electrolyte was prepared by dissolving 1 M $Zn(OH)_2$ in 4 M NaOH.

Electrodes for flow battery cell tests were carbon papers (SGL 39AA) baked at 400 °C overnight. Electrodes for electrodeposition battery tests were 1 mm thick carbon cloths.

Cell cycling

Cycling of $Fe(Bhmbpy)_3$/BTMAPAQ cell was conducted in a 5 cm^2 flow battery, using 5 mL 0.1 M $Fe(Bhmbpy)_3$ as capacity limiting side, pairing with 10 mL 0.1 M negolyte. Electrolyte compositions are described in Materials and Synthesis without further treatment before usage. Electrolytes were pumped using a flow rate of 60 mL/min through 3 layers of baked carbon papers as electrodes. A Selemion DSV-N was used as the AEM. pH sensors were inserted in posolyte and negolyte. pH reading out was collected by an Arduino during cell operation and manually calibrated after. The cell was operated with a constant current (40 mA cm^{-2}) followed by constant potentials of 1.75 V (charging) and 0.4 V (discharging). During charging, the potential was held until the current density dropped lower than 5 mA cm^{-2}. During discharge, the current density cutoff was 1 mA cm^{-2} to ensure full discharge of the iron complex and its dimers. During operation, we would bubble air through the negolyte if the cell was out of balance.

Cycling of DPPEAQ/NaBr cell used 5 mL DPPEAQ electrolyte and 10 mL NaBr and Nafion 212 as the CEM, with other conditions the same as the $Fe(Bhmbpy)_3$/BTMAPAQ cell. Cut-off voltage was set as 2 V and 0.7 V with cut-off current density of 10 mA cm^{-2} and 5 mA cm^{-2}, for charge and discharge respectively.

Cell polarization

The full accessed capacity of the cell was first determined by performing a full charge/discharge cycling, which was accomplished by applying constant current followed by potential holds until the current decreased to the cutoff value. For semi-solid ARFBs, accessible capacity (100 SOC) was presumed to be 10 mAh cm^{-2}. The cell was then charged with intervals to various states of charge (calculated from the percentage of the total accessed capacity). To determine the high-frequency area-specific resistance (ASR), electrochemical impedance spectroscopy (EIS) measurements were conducted at each SOC with a perturbation of 10 mV and frequencies ranging from 1 to 100,000 Hz. The battery's open-circuit voltage (OCV) was also measured. Additionally, the potential was swept at each SOC at a scan rate of 100 mV s^{-1}, and the current response as a result was measured to create polarization curves. The polarization ASR was computed using the linear region of the polarization curves near OCV.

For galvanostatic tests, constant current densities between 20 to 80 mA cm^{-2} were applied during both charge and discharge cycles. Only $Fe(Bhmbpy)_3$/BTMAPAQ cell used potential holds during discharge. Consequently, the Coulombic, capacity utilization and energy efficiencies are calculated for each current density.

Supplementary notes

Supplementary Note. 1: Crossover of acid-base in a single-membrane pH-decoupling ARFB[1]

Crossover flux can be expressed by **Equation S1**. $[H^+]_p$, $[H^+]_n$ represent the proton concentrations in posolyte and negolyte, respectively. $[OH^-]_p$, $[OH^-]_n$ represent the hydroxide concentrations in posolyte and negolyte, respectively. l_{AEM} represents the thickness of AEM. j represents the signed ionic current, with direction pointing from posolyte to negolyte as positive. P represents the permeability coefficient of ions though the membrane. M represents the ion-migration coefficient inside the membrane due to the applied electric field. Specifically, the ion migration coefficients can be expressed as **Equation S2 – S3**. Here, D represents the diffusivity of an ion in a membrane. Z is the signed charge number of the ion. F is Faraday's constant. R is the universal gas constant and T is the absolute temperature. σ is the conductivity of the membrane in the electrolyte.

$$J_{crossover} = P_{H^+}^{AEM}\frac{[H^+]_p - [H^+]_n}{l_{AEM}} + M_{H^+}^{AEM} j + P_{OH^-}^{AEM}\frac{[OH^-]_n - [OH^-]_p}{l_{AEM}} + M_{OH^-}^{AEM} j \tag{S1}$$

$$M_{H^+}^{AEM} = D_{H^+}^{AEM}[H^+]_{AEM}\frac{ZF}{\sigma^{AEM}RT} \tag{S2}$$

$$M_{OH^-}^{AEM} = D_{OH^-}^{AEM}[OH^-]_{AEM}\frac{ZF}{\sigma^{AEM}RT} \tag{S3}$$

With a CEM setup, the crossover is described in **Equation S4 – S6**.

$$J_{crossover} = P_{OH^-}^{CEM}\frac{[OH^-]_n - [OH^-]_p}{l_{CEM}} + M_{OH^-}^{CEM} j + P_{H^+}^{CEM}\frac{[H^+]_p - [H^+]_n}{l_{CEM}} + M_{H^+}^{CEM} j \tag{S4}$$

$$M_{OH^-}^{CEM} = D_{OH^-}^{CEM}[OH^-]_{CEM}\frac{ZF}{\sigma^{CEM}RT} \tag{S5}$$

$$M_{H^+}^{CEM} = D_{H^+}^{CEM}[H^+]_{CEM}\frac{ZF}{\sigma^{CEM}RT} \tag{S6}$$

In these equations, crossover of protons through AEMs and hydroxide through CEMs have been described in our previous work. The crossover (exchange) of protons through CEMs and hydroxide through AEMs can be estimated as **Equation S7 – S12**. K_X^Y is the conductivity of Z charged ion X in membrane Y.

For protons through CEMs:

$$J_{protons,CEM} \approx M_{H^+}^{CEM} j \tag{S7}$$

$$M_{H^+}^{CEM} \approx \frac{[H^+]_p K_{H^+}^{CEM}}{[H^+]_p K_{H^+}^{CEM} + \sum z[other\ cations^{z+}]_p K_{other\ cations^{z+}}^{CEM}} \tag{S8}$$

For hydroxide through AEMs:

$$J_{hydroxides,AEM} \approx M_{OH^-}^{AEM} j \quad \text{(S9)}$$

$$M_{OH^-}^{AEM} \approx \frac{[OH^-]_n K_{OH^-}^{AEM}}{[OH^-]_n K_{OH^-}^{AEM} + \sum z[other\ anions^{z-}]_n K_{other\ anions^{z-}}^{AEM}} \quad \text{(S10)}$$

For protons through AEMs:

$$J_{protons,AEM} \approx P_{H^+}^{AEM} \frac{[H^+]_p - [H^+]_n}{l_{AEM}} \quad \text{(S11)}$$

For hydroxides through CEMs:

$$J_{hydroxides,CEM} \approx P_{OH^-}^{CEM} \frac{[OH^-]_n - [OH^-]_p}{l_{CEM}} \quad \text{(S12)}$$

For example, in the case of $Fe(Bhmbpy)_3$/BTMAPAQ cell, the acid crossover flux from pH 2 – 4 buffer solution was extracted from reported data,[1] determined to be lower than 1 nmol s^{-1} cm^{-2}. The hydroxide crossover flux from pH 12 solution was estimated using equation S11, because the conductivity of hydroxide and chloride anions are similar in Selemion DSV-N:

$$J_{hydroxides,AEM} \approx M_{OH^-}^{AEM} j \frac{0.01\ M}{=0.01M + 1M} * 40mA\ cm^{-2} \approx 4\ nmol\ s^{-1} cm^{-2} \quad \text{(S11)}$$

The number of moles of the acid-base crossover can be calculated as:

$$n_{net\ crossover} = AtJ_{crossover}$$

A is the membrane area, *t* is the charging/discharging duration.

The changing of acid/base concentration can be calculated as:

$$c_{net\ crossover} = n_{net\ crossover}/V$$

V is the volume of electrolyte. With a fixed charging/discharging current density, t/V is unchanged when only changing the volume of electrolyte. Therefore, the influence of acid-base crossover is decoupled from the electrolyte volume (total capacity).

Supplementary Note. 2: OER as proton sources for bromide posolyte

Oxygen evolution reaction (OER) requires a high potential (thermodynamically 1.23 V vs. RHE, with high overpotential of hundreds of millivolts), posing risk of over-oxidizing molecules. For example, iodine can be oxidized during OER:

$0.5I_2 + 3H_2O - 5e^- \rightarrow 6H^+ + IO_3^-$ $\phi = 1.2$ V vs. SHE, pH 0

Bhmbpy can be oxidized during OER or by oxidants[2]:

Bhmbpy + $H_2O - 2e^- \rightarrow 2H^+$ + Bhmpby-O

Owing to the high voltage of BrO_3^-/Br_2, with appropriate OER catalysts, OER can happen without driving unfavored irreversible oxidation of bromine:

$3Br^- - 2e^- \rightarrow Br_3^-$ $\phi = 1.09$ V vs. SHE, pH 0

$0.5Br_2 + 3H_2O - 5e^- \rightarrow 6H^+ + BrO_3^-$ $\phi = 1.5$ V vs. SHE, pH 0

$H_2O - 2e^- \rightarrow 2H^+ + 0.5\ O_2$ $\phi = 1.23$ V vs. SHE, pH 0

But anti-oxidation electrodes and buffers are required to avoid oxidation side reactions. PAA and acetate can be oxidized by bromine. Inorganic buffers like phosphate can be an alternative.

Supplementary Note. 3: BPM sub-cell for pH recovery in pH-decoupling electrodeposition batteries

Using the BPM sub-cell for pH-recovery has many benefits. Because electrolytes are discharged in the sub-cell, working voltage of the BPM cell will not post extra risks toward electrolyte decomposition. However, pumping electrolytes into the sub-cell for ex-situ pH recovery has an intrinsic requirement that both the oxidized and reduced form of the redox active molecule have to be soluble and flowable. This makes the sub-cell hard to be used in pH-decoupling electrodeposition batteries. For example, Zn and MnO_2 can hardly be pumped out into BPM cell to be discharged. Flowable redox mediators are required, in order to use BPM sub-cell for pH recovery in pH-decoupling electrodeposition batteries.

The solution to this problem is to introduce a low concentration of flowable redox couple. Flowable redox couples are actually already added in many electrodeposition batteries to increase the kinetics and reversibility of the cells. For example, people have developed using iodine for MnO_2 posolyte and flavin mononucleotide for polysulfide negolyte.

The same molecule can be added into both posolyte and negolyte, as long as it fits the requirements. The requirements of the adding flowable redox molecules are: 1. Low concentration. It cannot be the main redox couple that controls the charging and discharging of the cell. 2. Reversibility. The charging and discharging of the added molecules better not require large overpotential. 3. Compatible with the main redox couple. It cannot accelerate or cause decomposition of the original electrolyte. 4. Stability. The fade rate of itself should not be too high (> 0.1 %/day). 5. Suitable redox potential. This is the most important requirement. The potential of the added flowable redox molecules requires to be lower than the posolyte, but higher than the negolyte. In which case, during charging, the added molecules will become oxidized form in the posolyte and reduced form in the negolyte before charging of the main couples happen. Also, they will remain oxidized in the posolyte and reduced in the negolyte during cell cycling, because the cell does not have to hit the discharge voltage of the added couple. They can be discharged in the BPM sub-cell,

generating acid and base, and be oxidized/reduced back by chemical or electrochemical reactions in the main cell, mediating the acid-base generation by mediating the charge transfer from the main cell into sub-cell.

Supplementary Table

Supplementary Table S1: Redox molecule candidates**.**

Name & Structure	Voltage (V vs. SHE)	Working pH	Note	Reference
Ce_2O^{6+}/Ce^{3+}	1.81	< 0	Posolyte. Cation. Strong acid, need to consider acid crossover. Need to check water splitting.	[3]
Ce^{4+}/Ce^{3+}	1.44	< 0	Posolyte. Cation. Strong acid, need to consider acid crossover. Voltage changes with anions. Need to check water splitting.	[4]
Cl_2/Cl^-	1.36	< 7	Posolyte. Anion. High vapor pressure.	
MnO_2/Mn^{2+}	1.22 (pH = 0)	< 2	Posolyte. Cation. Strong acid, need to consider acid crossover. Proton coupled.	[5]
Br_3^-/Br^-	1.09	< 7	Posolyte. Anion. High vapor pressure.	[6]
VO_2^+/VO^{2+}	1.04 (pH = 0)	< 1	Posolyte. Cation. Strong acid, need to consider acid crossover. Proton coupled.	[7]
TEMPTMA 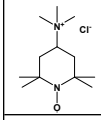	0.60	~ 7	Posolyte. Cation.	[8]
TEMPO-4-sulfate 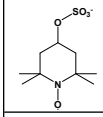	0.86	~7	Posolyte. Anion.	[9]
$Fe^{3+/2+}(Bhmbpy)_3$ 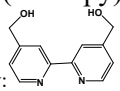 Bhmbpy:	0.98	2 – 4	Posolyte. Cation.	[2]
$Na_4[Fe^{3+/2+}(Dcbpy)_2(CN)_2]$ 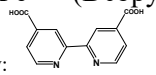 Dcbpy:	0.64	3 – 12	Posolyte. Anion.	[10]
$MnO_2/Mn(OAc)_2$	0.85	4	Posolyte. Cation.	[11]
TMAP-TEMPO	0.80	~ 7	Posolyte. Cation.	[12]

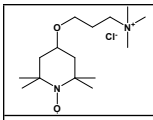				
4-OH-TEMPO 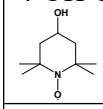	0.81	~ 7	Posolyte. Cation.	13
Fe^{3+}/Fe^{2+}	0.77	< 3	Posolyte. Cation.	14
FcNCl ($Fe^{3+/2+}$) 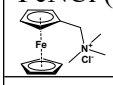	0.61	~ 7	Posolyte. Cation.	
Fc-SO_3Na 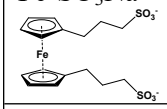	0.3	~ 7	Posolyte. Anion.	15
I_3^-/I^-	0.54	< 7	Posolyte. Anion.	16
Fc⊂β-CD ($Fe^{3+/2+}$) 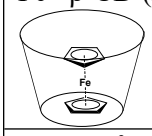	0.5	~ 7	Posolyte. Cation.	17
$Fe(CN)_6^{3-}$/ $Fe(CN)_6^{4-}$	0.4	> 7	Posolyte. Anion.	
BTMAP-Fc ($Fe^{3+/2+}$) 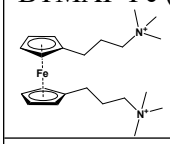	0.39	~ 7	Posolyte. Cation.	18
Fe(citrate)/ Fe(citrate)$^-$	0	~ 3.5	Anion.	19
S_4^{2-}/S_2^{2-}	−0.42	> 11	Negolyte. Anion.	20
BPP-Vi 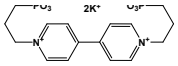	−0.46	~ 7	Negolyte. Anion.	21
2,6-DBEAQ 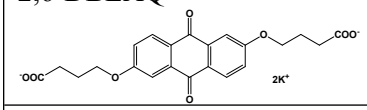	−0.52 (pH 12)	> 12	Negolyte. Anion.	22
2,6-DPPEAQ 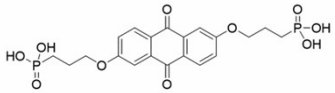	−0.50 (pH 12)	> 7	Negolyte. Anion.	23
DHAQ 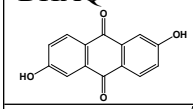	−0.68 (pH 14)	14	Negolyte. Anion.	24
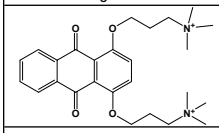	−0.55 (pH 12)	> 7	Negolyte. Cation. Proton coupled when pH < 12.	9
BHPC 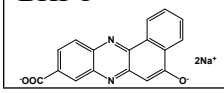	−0.78 (pH 14)	> 12	Negolyte. Anion. Proton coupled.	25

DHPS 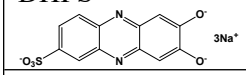	−1.05 (pH 14)	> 13	Negolyte. Anion. Proton coupled.	26
1,8-PFP 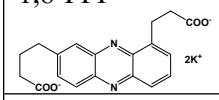	−0.57 (pH 14)	> 7	Negolyte. Anion. Proton coupled.	27
7,8-hydroxyalloxazine 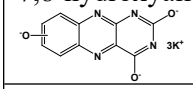	−0.72 (pH 14)	14	Negolyte. Anion. Proton coupled.	28
$Fe^{3+/2+}$(TEOA) 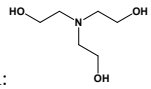 TEOA:	−0.78	13	Negolyte. Anion.	19
Methyl viologen 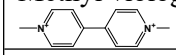	−0.42	~ 7	Negolyte. Cation.	13
BTMAP-Vi 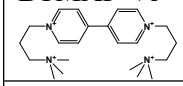	−0.40	~ 7	Negolyte. Cation.	18
Diquat 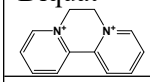	−0.37	~ 7	Negolyte. Cation.	29
$[(NPr)_2PV]$-4Cl 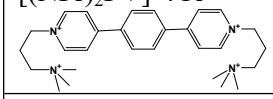	−0.78	~ 7	Negolyte. Cation.	30
$Fe^{3+/2+}$(DIPSO) 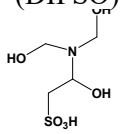 DIPSO:	−0.82	> 13	Negolyte. Anion.	31
$Cr^{3+/2+}$ (PDTA) 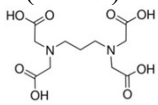 PDTA:	−1.18	~ 9	Negolyte. Anion. Need to check water splitting.	32
$Zn/Zn(OH)_4^{2-}$	−1.22 (pH 14)	> 14	Negolyte. Anion. Strong base. Need to consider base crossover. Need to check water splitting.	33

Supplementary Table S2: Potential proton pumps**.** Any oxidation half-reaction may be paired with any reduction half-reaction. The last entry is a full reaction.

Reaction	Potential, V vs. RHE	Type	Note
Hydrogen evolution reaction (HER)	0	Reduction, hydroxide	Catalysts are not necessary. Be cautious of over-reduction of molecules. Some redox

$2H_2O + 2e^- \rightarrow H_2 + 2OH^-$		source	couples have this side reaction occurring spontaneously.[4,32]
Hydrogen oxidation reaction (HOR) $H_2 - 2e^- \rightarrow 2H^+$	0	Oxidation, proton source	Catalysts and hydrogen gas are required. Be cautious of decomposition of molecules on HOR catalysts. Usually *ex-situ*.
Oxygen evolution reaction (OER) $2H_2O - 4e^- \rightarrow O_2 + 2H^+$	1.23	Oxidation, proton source	Catalysts may be required because of bad kinetics. Be cautious of oxidation of carbon electrodes and molecules. Some redox couples have this side reaction occurring spontaneously.[34]
Oxygen reduction reaction (ORR, 2e) $H_2O + O_2 + 2e^- \rightarrow HO_2^- + OH^-$ (pKa of H_2O_2 is about 11.7)	0.68 (pH < 12)	Reduction, hydroxide source	Usually spontaneous when introducing air into the negolyte. The amount of air introduced should be controlled.
Oxygen reduction reaction (ORR, 4e) $2H_2O + O_2 + 4e^- \rightarrow 4OH^-$	1.23	Reduction, hydroxide source	Usually spontaneous when introducing air into the negolyte. The amount of air introduced should be controlled.
BPM: $H_2O \rightarrow H^+$ (pH 0) + OH^- (pH 14)	0.83 V, full cell	Water dissociation, source of protons and hydroxide	Must be *ex-situ* in a sub-cell. Flowable mediators must be introduced when working on electrodeposition batteries. Driven by discharging of the electrolytes.

Supplementary figures

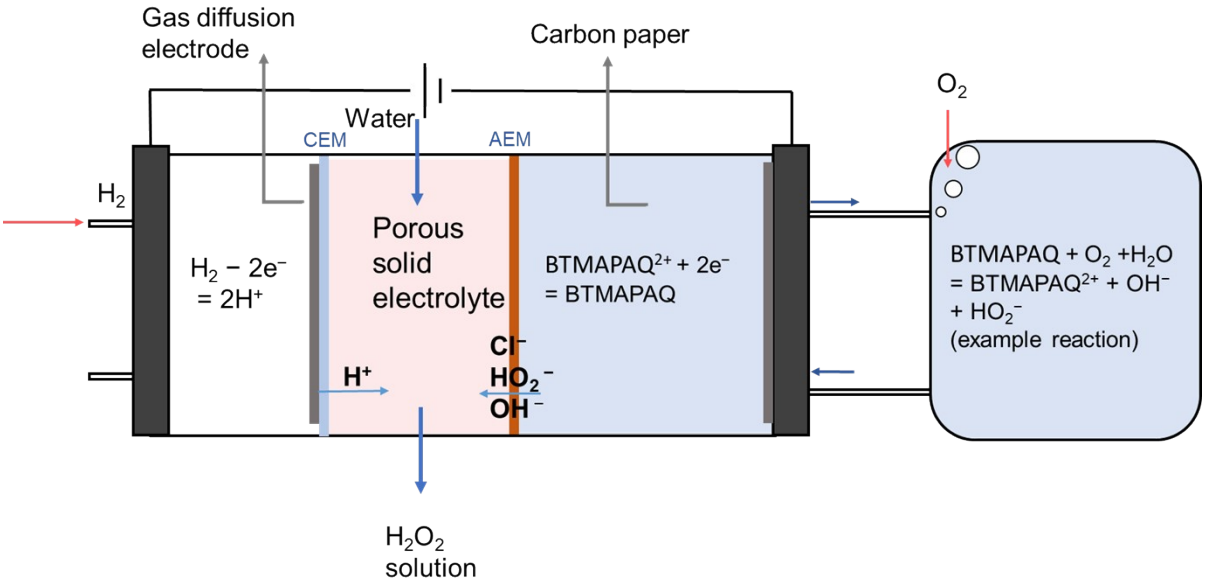

Supplementary Fig. S1 | Cell structure of H_2O_2 production using BTMAPAQ mediated ORR. The formation of H_2O_2 in the center chamber suggests the formation and electromigration of HO_2^-.

The support the generation and migration of HO_2^-, we assembled a three-chamber, two-membrane electrochemical cell,[35] as shown in **Supplementary Fig. S1**. The cell was operated under a constant current of 20 mA cm^{-2}. Air was continuously bubbled through the BTMAPAQ catholyte (0.2 M, 5 mL). With this setup, we collected the solution exiting the center chamber and detected the formation of H_2O_2. We used $KMnO_4$ to titrate the solution to determine the molarity of the generated hydrogen peroxide. The Faradaic efficiency (FE) of the 2e ORR reaction was calculated using the following equation, where n_{H2O2} stands for the molarity of the obtained H_2O_2. F is the Faradaic constant. Q is the charge passing through the circuit.

$$FE = n_{H2O2} * 2 * F/Q$$

The Faradaic efficiency was about 3% – 8% when the system reached a steady state, which we interpret as the formation and electromigration of HO_2^- through the AEM.

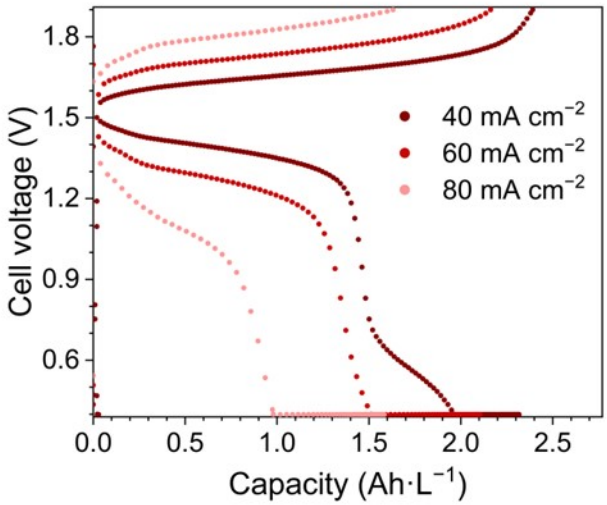

Supplementary Fig. S2 | Galvanostatic tests for the Fe(Bhmbpy)$_3$/BTMAPAQ cell at 40, 60 and 80 mA cm^{-2}. Theoretical capacity is about 2.77 Ah L^{-1}. Cutoff voltage is 1.9 V, and 0.4 V for charging and discharging. Voltage hold was applied during discharge until current dropping lower than 1 mA cm^{-2}. Dimerization and ligand self-oxidation of Fe(Bhmbpy)$_3$ make the cell hardly practicable.

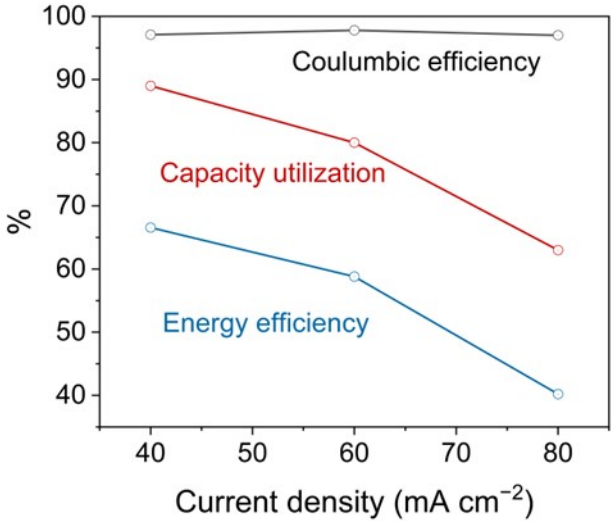

Supplementary Fig. S3 | Capacity utilization and Coulombic and round-trip energy efficiencies vs. applied current density for the Fe(Bhmbpy)$_3$/BTMAPAQ cell during galvanostatic tests.

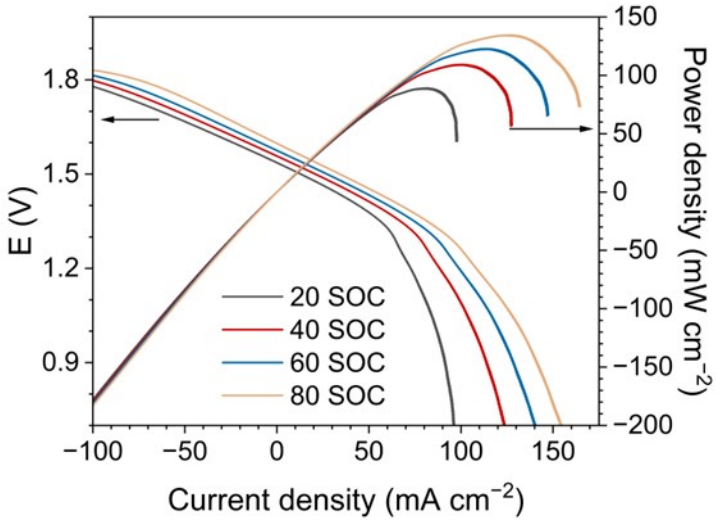

Supplementary Fig. S4 | Cell voltage and power density during discharge of the Fe(Bhmbpy)$_3$/BTMAPAQ cell at different states of charge. Power density is not high mainly due to the mass transport limitation.

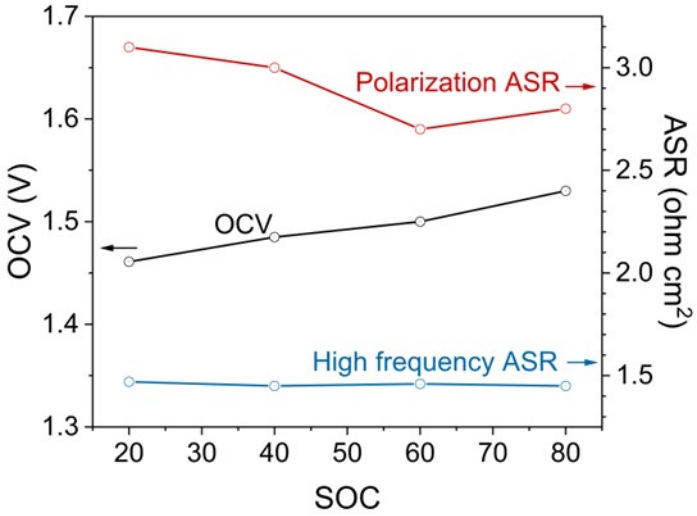

Supplementary Fig. S5 | Dependence on SOC of OCV and ASR near OCV for the Fe(Bhmbpy)$_3$/BTMAPAQ cell. Ohmic resistance and charge transfer resistance can also be further engineered for a higher power.

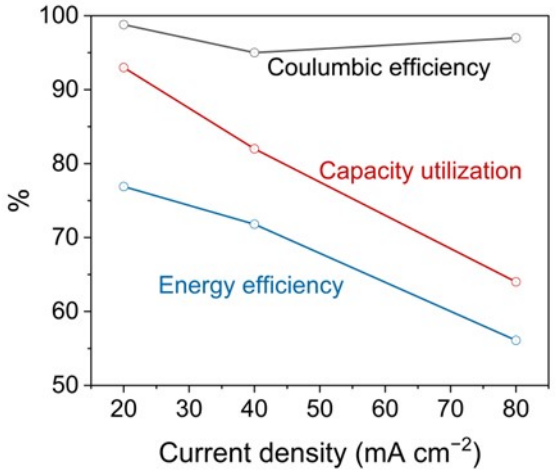

Supplementary Fig. S6 | Capacity utilization and Coulombic and round-trip energy efficiencies vs. applied current density for the NaBr/DPPEAQ cell during galvanostatic tests. Bromine and crossover of bromine oxidizes the membrane, electrode, buffer and DPPEAQ making the cell hardly practicable.

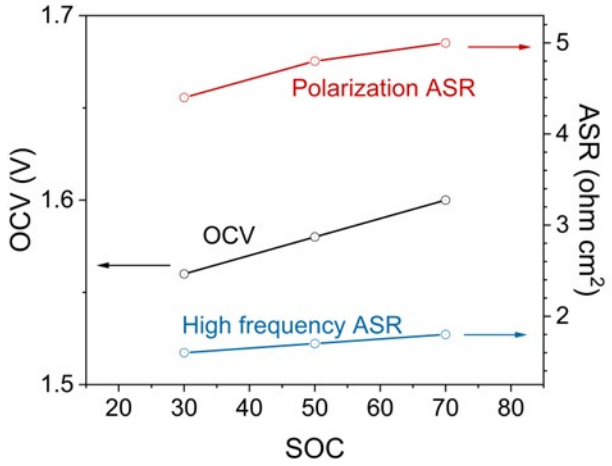

Supplementary Fig. S7 | Dependence on SOC of OCV and ASR near OCV for the NaBr/DPPEAQ cell.

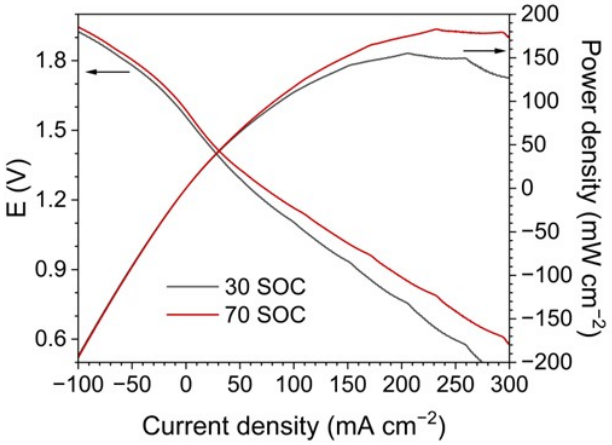

Supplementary Fig. S8 | Cell voltage and power density during discharge of the NaBr/DPPEAQ cell at different states of charge. Power density is not high mainly due to high ohmic resistance of the cell and slow kinetic of NaBr-$NaBr_3$ couple.

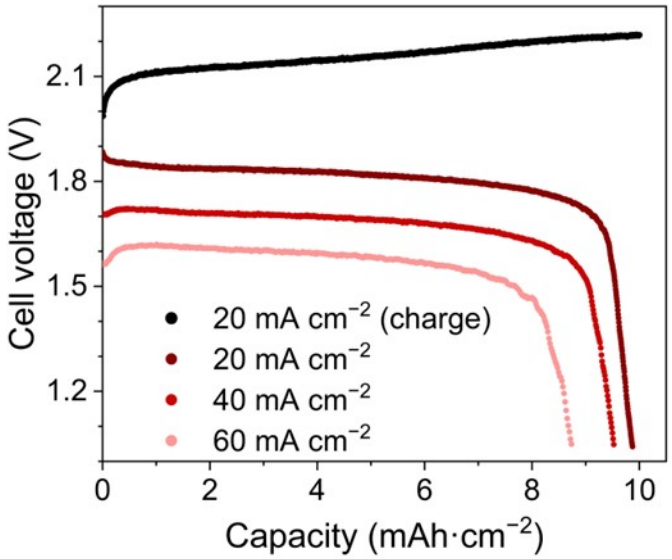

Supplementary Fig. S9 | Galvanostatic tests for the $Mn(OAc)_2/Na_2Zn(OH)_4$ cell at 20, 40, 60 and 80 mA cm^{-2}. Charging capacity is set as 10 mAh cm^{-2}. Cutoff voltage is 1.0 V for discharging. Crossover of Mn ions, Zn ions, dendrites formation and oxidation of acetates when applying OER for pH recovery making the cell hardly practicable.

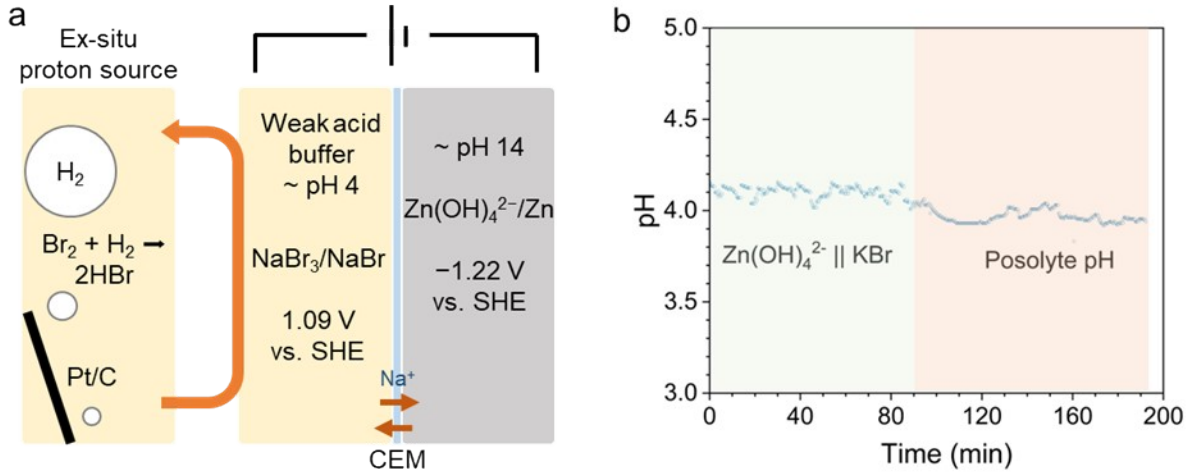

Supplementary Fig. S10 | Hydrogen oxidation as proton generator. a, A schematic of the system. Bromine was used as the flowable posolyte. HOR was catalyzed by a commercial Pt GDE. **b,** pH of the posolyte bromine/bromide side (green shaded) after introducing hydrogen (red shaded). pH of the buffered posolyte went lower due to the generation of protons.

References for Supplementary Information

1. D. Xi, A. M. Alfaraidi, J. Gao, T. Cochard, L. C. I. Faria, Z. Yang, T. Y. George, T. Wang, R. G. Gordon, R. Y. Liu and M. J. Aziz, *Nat. Energy*, 2024, DOI: 10.1038/s41560-024-01474-1.
2. J. Gao, K. Amini, T. Y. George, Y. Jing, T. Tsukamoto, D. Xi, R. G. Gordon and M. J. Aziz, *Adv. Energy Mater.*, 2022, **12**.
3. S. Gu, K. Gong, E. Z. Yan and Y. Yan, *Energy Environ. Sci.*, 2014, **7**, 2986-2998.
4. P. K. Leung, C. Ponce-de-León, C. T. J. Low, A. A. Shah and F. C. Walsh, *J. Power Sources*, 2011, **196**, 5174-5185.
5. C. Zhong, B. Liu, J. Ding, X. Liu, Y. Zhong, Y. Li, C. Sun, X. Han, Y. Deng, N. Zhao and W. Hu, *Nat. Energy*, 2020, **5**, 440-449.
6. B. Huskinson, M. P. Marshak, C. Suh, S. Er, M. R. Gerhardt, C. J. Galvin, X. Chen, A. Aspuru-Guzik, R. G. Gordon and M. J. Aziz, *Nature*, 2014, **505**, 195-198.
7. G.-M. Weng, C.-Y. V. Li and K.-Y. Chan, *Materials Today Energy*, 2018, **10**, 126-131.
8. T. Janoschka, N. Martin, M. D. Hager and U. S. Schubert, *Angewandte Chemie International Edition*, 2016, **55**, 14427-14430.
9. J. Winsberg, C. Stolze, A. Schwenke, S. Muench, M. D. Hager and U. S. Schubert, *ACS Energy Lett.*, 2017, **2**, 411-416.
10. X. Li, P. Gao, Y.-Y. Lai, J. D. Bazak, A. Hollas, H.-Y. Lin, V. Murugesan, S. Zhang, C.-F. Cheng and W.-Y. Tung, *Nat. Energy*, 2021, **6**, 873-881.
11. J. Lei, Y. Yao, Y. Huang and Y.-C. Lu, *ACS Energy Lett.*, 2022, **8**, 429-435.
12. Y. Liu, M.-A. Goulet, L. Tong, Y. Liu, Y. Ji, L. Wu, R. G. Gordon, M. J. Aziz, Z. Yang and T. Xu, *Chem*, 2019, **5**, 1861-1870.
13. T. Liu, X. Wei, Z. Nie, V. Sprenkle and W. Wang, *Adv. Energy Mater.*, 2016, **6**, 1501449.
14. K. Gong, X. Ma, K. M. Conforti, K. J. Kuttler, J. B. Grunewald, K. L. Yeager, M. Z. Bazant, S. Gu and Y. Yan, *Energy Environ. Sci.*, 2015, **8**, 2941-2945.
15. J. Yu, M. Salla, H. Zhang, Y. Ji, F. Zhang, M. Zhou and Q. Wang, *Energy Storage Materials*, 2020, **29**, 216-222.
16. M. Mousavi, H. Dou, H. Fathiannasab, C. J. Silva, A. Yu and Z. Chen, *Chem. Eng. J.*, 2021, **412**, 128499.
17. Y. Li, Z. Xu, Y. Liu, S. Jin, E. M. Fell, B. Wang, R. G. Gordon, M. J. Aziz, Z. Yang and T. Xu, *ChemSusChem*, 2021, **14**, 745-752.
18. E. S. Beh, D. De Porcellinis, R. L. Gracia, K. T. Xia, R. G. Gordon and M. J. Aziz, *ACS Energy Lett.*, 2017, **2**, 639-644.
19. K. Gong, F. Xu, J. B. Grunewald, X. Ma, Y. Zhao, S. Gu and Y. Yan, *ACS Energy Lett.*, 2016, **1**, 89-93.
20. J. Lei, Y. Zhang, Y. Yao, Y. Shi, K. L. Leung, J. Fan and Y.-C. Lu, *Nat. Energy*, 2023, DOI: 10.1038/s41560-023-01370-0, 1-10.
21. S. Jin, E. M. Fell, L. Vina-Lopez, Y. Jing, P. W. Michalak, R. G. Gordon and M. J. Aziz, *Adv. Energy Mater.*, 2020, **10**.
22. D. G. Kwabi, K. Lin, Y. Ji, E. F. Kerr, M.-A. Goulet, D. De Porcellinis, D. P. Tabor, D. A. Pollack, A. Aspuru-Guzik, R. G. Gordon and M. J. Aziz, *Joule*, 2018, **2**, 1894-1906.
23. Y. Ji, M. A. Goulet, D. A. Pollack, D. G. Kwabi, S. Jin, D. Porcellinis, E. F. Kerr, R. G. Gordon and M. J. Aziz, *Adv. Energy Mater.*, 2019, **9**.
24. K. Lin, Q. Chen, M. R. Gerhardt, L. Tong, S. B. Kim, L. Eisenach, A. W. Valle, D. Hardee, R. G. Gordon and M. J. Aziz, *Science*, 2015, **349**, 1529-1532.

25. C. Wang, X. Li, B. Yu, Y. Wang, Z. Yang, H. Wang, H. Lin, J. Ma, G. Li and Z. Jin, *ACS Energy Lett.*, 2020, **5**, 411-417.
26. A. Hollas, X. Wei, V. Murugesan, Z. Nie, B. Li, D. Reed, J. Liu, V. Sprenkle and W. Wang, *Nat. Energy*, 2018, **3**, 508-514.
27. J. Xu, S. Pang, X. Wang, P. Wang and Y. Ji, *Joule*, 2021, **5**, 2437-2449.
28. K. Lin, R. Gómez-Bombarelli, E. S. Beh, L. Tong, Q. Chen, A. Valle, A. Aspuru-Guzik, M. J. Aziz and R. G. Gordon, *Nat. Energy*, 2016, **1**.
29. J. Huang, Z. Yang, V. Murugesan, E. Walter, A. Hollas, B. Pan, R. S. Assary, I. A. Shkrob, X. Wei and Z. Zhang, *ACS Energy Lett.*, 2018, **3**, 2533-2538.
30. M. Pan, Y. Lu, S. Lu, B. Yu, J. Wei, Y. Liu and Z. Jin, *ACS Appl. Mater. Interfaces*, 2021, **13**, 44174-44183.
31. M. Shin, C. Noh, Y. Chung and Y. Kwon, *Chem. Eng. J.*, 2020, **398**.
32. B. H. Robb, J. M. Farrell and M. P. Marshak, *Joule*, 2019, **3**, 2503-2512.
33. F. Yu, L. Pang, X. Wang, E. R. Waclawik, F. Wang, K. K. Ostrikov and H. Wang, *Energy Storage Materials*, 2019, **19**, 56-61.
34. T. Kong, J. Liu, X. Zhou, J. Xu, Y. Xie, J. Chen, X. Li and Y. Wang, *Angew. Chem. Int. Ed.*, 2023, **62**, e202214819.
35. C. Xia, Y. Xia, P. Zhu, L. Fan and H. Wang, *Science*, 2019, **366**, 226-231.